

# Numerical study of turbulent trailing-edge flows with base cavity effects using URANS

Thau Do<sup>a</sup>, Li Chen<sup>b,\*</sup>, Jiyuan Tu<sup>a</sup>

<sup>a</sup>*School of Aerospace, Mechanical and Manufacturing Engineering, RMIT University, P.O. Box 71, Bundoora, Vic. 3083, Australia*

<sup>b</sup>*Maritime Platform Division, Defence Science & Technology Organisation, P.O. Box 4331, Melbourne, Vic. 3001, Australia*

Received 29 July 2008; accepted 29 July 2010

Available online 16 September 2010

---

## Abstract

Turbulent flows over lifting surfaces exhibiting trailing-edge vortex shedding often cause adverse and complex phenomena, such as self-induced vibration and noise. In this paper, a numerical study on flow past a blunt-edged two-dimensional NACA 0015 section and the same section with various base cavity shapes and sizes at high Reynolds numbers has been performed using the unsteady Reynolds-averaged Navier–Stokes (URANS) approach with the realisable  $\kappa$ – $\epsilon$  turbulence model. The equations are solved using the control volume method of second-order accuracy in both spatial and time domains. The assessment of the application of URANS for periodic trailing-edge flow has shown that reasonable agreement is achieved for both the time-averaged and fluctuating parameters of interest, although some differences exist in the prediction of the near-wake streamwise velocity fluctuation magnitudes. The predicted Strouhal numbers of flows past the squared-off blunt configuration with varying degrees of bluntness agree well with published experimental measurements. It is found that the intensity of the vortex strengths at the trailing-edge is amplified when the degree of bluntness is increased, leading to an increase in the mean square pressure fluctuations. The numerical prediction shows that the presence of the base cavity at the trailing-edge does not change the inherent Strouhal number of the 2D section examined. However, it does have an apparent effect on the wake structure, local pressure fluctuations and the lift force fluctuations. It is observed that the size of the cavity has more influence on the periodic trailing-edge flow than its shape does.

Crown Copyright © 2010 Published by Elsevier Ltd. All rights reserved.

*Keywords:* Trailing-edge flow; Vortex shedding; Base cavity; Unsteady RANS

---

## 1. Introduction

Blunt-edged aerofoils or hydrofoils submerged in high Reynolds number turbulent flows often exhibit undesirable self-induced discrete tonal noise. The presence of the blunt trailing-edge induces a periodic vortex shedding phenomenon, causing fluctuations of the surface pressures, which can lead to self-sustained structural vibrations as well as change the magnitude and spectrum of the acoustic energy at the trailing-edge (Bourgoyne et al., 2000). The control of this vortex shedding has inspired many experimental and numerical studies in this field over the last decade. For example, very high Reynolds number flows over a hydrofoil were studied experimentally by Bourgoyne et al. (2003, 2005) and numerically

---

\*Corresponding author. Tel: +61 3 96268220; fax: +61 3 96268999.

E-mail address: li.chen@dsto.defence.gov.au (L. Chen).

Nomenclature			
		$C_d$	drag force coefficient, $F_d/q_\infty C$
		$C_l$	lift force coefficient, $F_l/q_\infty C$
$A_c$	characteristic cavity area as defined in Table 1	$C_p$	pressure coefficient, $p/q_\infty C$
$A_h$	reference cavity area, $h \times h$	$l_f$	wake formation length
$C$	chord length	$y_f$	cross-wake shear layer thickness
$h$	trailing-edge height	$U_\infty$	freestream velocity
$f$	frequency	$q_\infty$	dynamic pressure, $\rho U_\infty^2/2$
$l$	characteristic length scale	$St_l$	Strouhal number based on $l$ , $fl/U$
$p$	pressure	$Re_l$	Reynolds number based on $l$ , $(\rho U_\infty l)/\mu$
		$\delta^*$	displacement boundary layer thickness

by Date and Turnock (2002) and Paterson and Peltier (2005) to improve the understanding of the rich physics, and its association with the noise generation were investigated numerically and analytically by Blake (1975), Howe (1999, 2000, 2001) and Wang and Moin (2000). Recently, the self-sustained vibration of a NACA 0012 foil subjected to a low-to-moderate Reynolds number was studied experimentally by Poirel et al. (2008). Howe (1991) calculated the sound generated by an aerofoil of serrated trailing-edge analytically and concluded that a significant noise reduction was achieved with the serrated trailing-edge. Blake (1986) comprehensively reviewed experimental data of various studies and concluded that turbulent flow-induced tonal noise can be eliminated by making the trailing-edge sufficiently sharp. However, due to manufacturing limitations and the structural requirement for aerofoils to withstand tremendous lift and drag forces, especially for hydrodynamic applications, the enclosure of the trailing-edge always results in a certain degree of bluntness in practice. This dilemma represents a challenge for marine and aerospace engineers alike, in minimising tonal noise emissions and preventing fatigue failure caused by coincidences of the vortex shedding frequency and the natural frequency of the structure.

The understanding of bluff-body wake dynamics has improved significantly due to the rapid development of advanced experimental and numerical techniques over the last two decades (Williamson, 1996). However, it cannot be directly applied to the near-wake of a streamline body because of differences between the two wake dynamics, such as the larger distance between the front and rear stagnation points and the stronger dependence on the rear geometry for a streamline body wake (Bourgoyne et al., 2005). Blake (1975) carried out aerodynamic and hydrodynamic surveys of the wake dynamical characteristics of a simple symmetric aerofoil (referred as a lifting strut) with a squared-off blunt trailing-edge that exhibits vortex shedding, using techniques proposed by Bearman (1965). The subsequent studies by Blake (1976), Blake et al. (1977) and Gershfeld et al. (1988) used these inherent wake characteristics, in particular the vortex formation length ( $l_f$ ), cross-wake shear layer thickness ( $y_f$ ) and trailing-edge pressure fluctuations, in the prediction of mode displacement amplitudes, location of the vortices and the acoustic spectrum in the immediate wake region. Recently, Bourgoyne et al. (2005) conducted an experimental study of the vortex shedding from an asymmetrical NACA 0016 with  $45^\circ$  and  $60^\circ$  apex angles. They confirmed that the vortex strength was controlled by the vertical velocity fluctuation near the trailing-edge and a strong vortex shedding occurred when the trailing-edge was sufficiently blunt. However, to the best of the authors' knowledge such information has been limited, even more so for the conventional streamlined and symmetrical hydrofoils containing a blunt trailing-edge. The inadequate literature available prevents generalisation of the behaviour of such wake characteristics across different sections and trailing-edge profiles, when different flow conditions are imposed. Further, more questions remain as to how these wake length scales, the Strouhal number and the intensity of the surface pressure fluctuations vary with the trailing-edge Reynolds number ( $Re_h$ ) for a particular trailing-edge configuration.

The influence of a trailing-edge cavity on the vortex-induced structural vibration of two-dimensional thick flat plates (with circular leading edge) has been extensively studied [see, e.g., Donaldson, 1956, Heskestad and Olberts, 1960, Toebes and Eagleson, (1961)]. It is clear from these studies that the presence of the cavity leads to a change in the vibration amplitudes relative to the basic squared-off blunt configuration. Heskestad and Olberts (1960) explained that the bound circulation strength (about the section) is reduced to account for the rotational fluid trapped inside the cavity, hence resulting in a reduction of the exciting lift force. On the other hand, the influence of the cavity on the shedding frequency is less certain. Toebes and Eagleson (1961) compared a section with a squared-off blunt trailing-edge and the same section containing a triangular cavity, while Zhdanov and Eckelmann (1994) examined a squared-off blunt profile and various rectangular cavity profiles, both studies reported that the shedding frequencies were altered. The change reported by Toebes and Eagleson (1961) was very small. However, Heskestad and Olberts (1960) observed an unchanged vortex shedding frequency for the comparison between a section with a squared-off blunt trailing-edge and the same section with a semicircular cavity. It is the intention of this work to use numerical methods to re-examine

the topic and to investigate whether the shedding frequency and the trailing-edge fluctuating pressure are modified when different cavity shapes are applied at the trailing-edge of the two-dimensional NACA 0015 section.

With the rapid advancement of computing power and the high-level maturity of numerical methods, the application of computational fluid dynamics (CFD) to engineering research and design has become the norm. Many commercially available packages, such as FLUENT and CFX, and the open source OPENFOAM are all using the same well-established numerical methods and providing the same widely used turbulence models. Applications of commercially available packages in both scientific researches and industrial designs can be found in many literatures [e.g., Mathey, 2008, Yang et al. 2008, Rani et al. (2007)]. With a thorough validation, the results obtained by either commercial package or the in-house code should have the same level of confidence. In this study, the commercial package FLUENT 6.2.16 is used to carry out all simulations. The numerical model is validated against available experimental data and subjected to a thorough mesh and time-step independent study.

It is generally accepted that the direct numerical simulation (DNS) is more accurate. However, it is still not feasible for many practical problems, particularly for complex high Reynolds number ( $Re$ ) wall-bounded flows (Rumsey and Ying, 2002), where the number of grid points required to resolve all scales of turbulence increases approximately as  $Re^3$  (Rodi, 1993). Large eddy simulation (LES) has emerged as a promising approach to numerical simulations of high Reynolds number flows, where the small scale turbulence or eddies are filtered, with only larger ones explicitly resolved while the effect of the smaller ones are modelled. Nevertheless, as pointed out by Iaccarino et al. (2003), LES still requires significantly fine spatial and temporal resolution, thus placing a high demand on both computing resources and time, despite the emergence of parallel computing.

Over the years, the Reynolds-averaged Navier–Stokes equation (RANS) has materialised as the most economical and efficient alternative for predicting high Reynolds number flows and is widely used in many engineering applications, with  $\kappa$ – $\epsilon$  being the most used turbulence model. Although the most advanced realisable  $\kappa$ – $\epsilon$  model is known to contain some deficiencies, it is the authors' intention to assess the unsteady performance of the blunt-edged NACA 0015 hydrofoil, rather than its absolute accuracy. To this end, numerical methods using RANS provide a time efficient and cost effective approach. Application of steady RANS with  $\kappa$ – $\epsilon$  turbulence model to the prediction of zero-pressure-gradient wakes of flat plates and two-dimensional lifting bodies is widespread; see for example Patel and Scheuerer (1982), Patel and Chen (1987), Tummers et al. (2007), Carlson et al. (2001), Nguyen and Gorski (1991) and Mulvany et al. (2004), all of which found this turbulence model predicts the near-wake features reasonably well compared to the experimental data. Moreover, a recent study by Iaccarino et al. (2003) claims that unsteady RANS (URANS) is highly capable of predicting flows with gross unsteadiness, given that the unsteadiness is deterministic and that the frequency spectrum shows a spike at the vortex shedding frequency. Yao et al. (2002) performed a direct comparison of URANS computation and DNS study of a low Reynolds number trailing-edge flow and concluded that although differences exist in the level of turbulence in the near-wake, many of the key flow features are predicted well by URANS. In light of this, the current work firstly aims to assess the capability of the URANS equations to predict two-dimensional high Reynolds number hydrofoil flows and its ability to capture the associated fluctuating unsteadiness in the near-wake. Secondly, it aims to provide a numerical investigation into the behaviour of near-wake flow characteristics, the Strouhal number and the intrinsic wake length scales for a symmetric NACA 0015 hydrofoil with trailing-edge Reynolds number and various modified trailing-edge profiles.

## 2. Numerical method

The two-dimensional NACA 0015 hydrofoil investigated has a chord length ( $C$ ) of 540 mm with a sharp trailing edge. The trailing-edge was modified into different geometric profiles as shown in Table 1, with profiles  $B$ ,  $C$  and  $D$  each containing a cavity. A characteristic cavity area,  $A_c$ , is defined as shown in Table 1. A parametric study based on varying the trailing-edge Reynolds number ( $Re_h$ ) was conducted with profile  $A$ . Variation of  $Re_h$  on this profile was achieved either by progressively truncating the two-dimensional section from 99.8% chord to 99.0% chord, thereby increasing the trailing-edge height while keeping the freestream velocity fixed at 5 m/s, or by keeping the trailing-edge height fixed at 2.08 mm while changing the velocity from 2.0 to 11.5 m/s, which corresponded to a Reynolds number variation between 1.407 and  $8.019 \times 10^6$ . The modified configurations of profiles  $B$ – $D$  were applied at 99% chord of the original sharp-edged section, resulting in a trailing-edge height of 3.58 mm. The two-dimensional section was aligned parallel to the oncoming flow, i.e. at zero angle of attack. Freestream turbulence intensity at the inlet was specified at 1%.

The computational domain developed for the URANS analysis of the NACA 0015 section were modelled as a free flow field having a two-dimensional  $C$ -type control volume of dimension:  $12C \times 4C$ . A *velocity inlet* boundary condition was applied 4 chord lengths upstream of the section's leading edge, while *symmetry* boundary condition was designated

Table 1  
Trailing-edge details and flow parameters of the two-dimensional NACA 0015 section.

Profile	$h$ (mm)	$A_c/A_h$	$Re_h$	Re	$U_\infty$ (m/s)
A <i>Squared-off Blunt</i>	2.08–3.58	–	5380–30,940	$1.407\text{--}8.019 \times 10^6$	2–11.5
B <i>90° Triangular Cavity</i>	3.58	0.25	23,180	$3.459 \times 10^6$	5
C <i>Semi-Circular Cavity</i>	3.58	0.39	23,180	$3.459 \times 10^6$	5
D <i>Rectangular Cavity</i>	3.58	0.25–1.18	23,180	$3.459 \times 10^6$	5

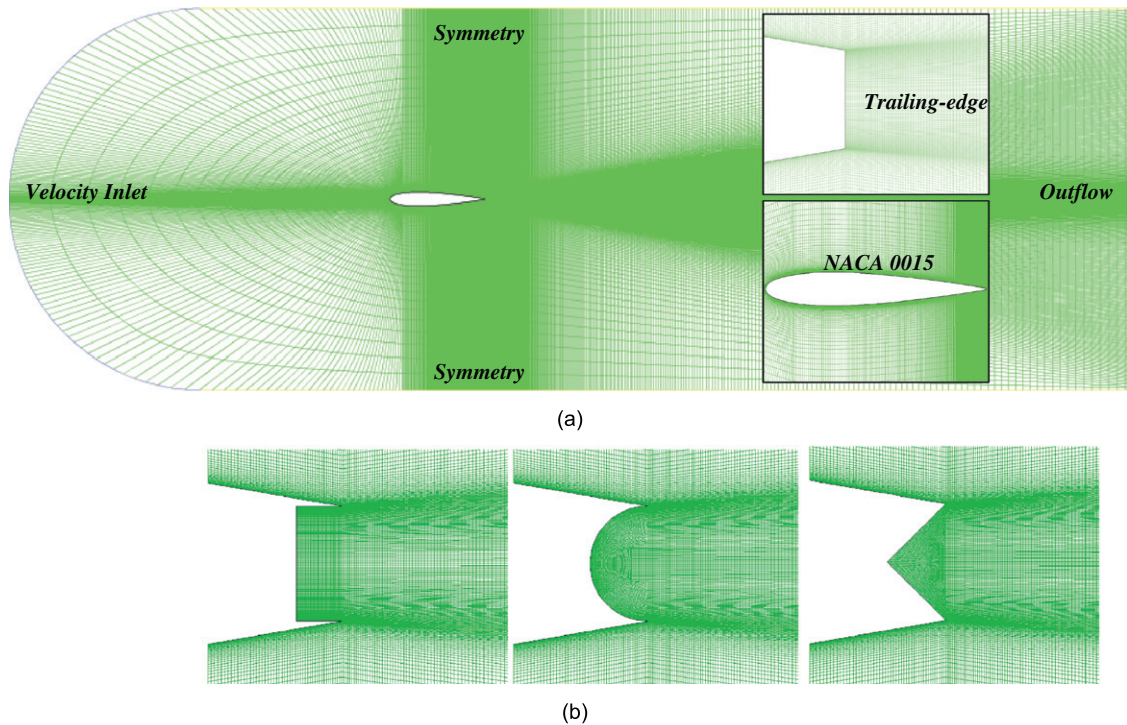


Fig. 1. A typical two-dimensional computational mesh and meshes around different trailing-edges.

at  $2C$  from the suction and pressure surface of the hydrofoil, which is considered sufficient far away from the foil to have little influence on the solution according to the simulation results obtained using a large domain of  $16C \times 8C$  and by Wang and Moin (2000) and Mulvany et al. (2004). The results of the large domain show little change in lift and drag coefficients. An outflow boundary condition was implemented at 7 chord lengths downstream of the trailing-edge. The surfaces of the lift section were defined with a no-slip *wall* boundary condition. The computational domain was discretized using pure quadrilateral cells with higher cell distribution allocated to the immediate wake region, as shown in Fig. 1(a).



The unsteady Reynolds-averaged Navier–Stokes equations (URANS) are discretised using the control volume approach and solved implicitly. To minimise the numerical diffusions, the second-order central differencing is used for diffusion term, a second-order upwind scheme is used for the convection term and a second-order accurate scheme is used for time domains. The pressure–velocity coupling is achieved by SIMPLE method. The turbulence of this high Reynolds number flow was modelled using the two-equation realisable  $\kappa$ – $\varepsilon$  model, following the findings reported by Mulvany et al. (2004). The model constants used in this study are the same as those used in Mulvany et al. (2004) unless it is defined explicitly. *Enhanced wall treatment with pressure gradient effects* was switched on to resolve the flow within the viscous sub-layer. In FLUENT, the enhanced wall treatment combines a two-layer model with a wall function accounting for the effects of compressibility, pressure gradient and heat transfer for both laminar and turbulent boundary layers. Selection of the real time-step ( $\Delta t$ ) for the resolution of the trailing-edge periodic flow was estimated using the residence time approach suggested by Shaw (1992) and successfully applied by Date and Turnock (2002). In this method, the time-step is equal to the distance of the smallest cell size in the wake region divided by the freestream velocity. The time-step size determined was then fixed throughout the entire simulation.

### 3. Results and discussion

#### 3.1. Validation of the URANS

Given that there is a lack of detailed experimental data for flow over the NACA 0015 section, the experimental data of a two-dimensional lifting strut (Blake, 1975) was used for the validation of URANS. The strut had a chord length of  $C = 508$  mm with a corresponding Reynolds number of  $Re = 1.06 \times 10^6$ . It has a circular leading edge followed by a flat section and was terminated with an adverse pressure gradient section having  $12.5^\circ$  included angle. The trailing-edge height was  $h = 14$  mm. Inflow turbulence intensity was measured at 2%, and the hydrofoil was aligned parallel to the incoming flow. This experiment was chosen as the validation case since this lifting strut is symmetrical, and contains a large aft section with adverse pressure gradient, replicating the nature of symmetrical aerofoils. Also, the ratio of the trailing-edge height to the maximum camber thickness is relatively low,  $h/h_{max} = 0.28$ .

The simulation was carried out with two meshes, 180,800 cells and 252,000 cells, which will be referred as mesh A and mesh B, respectively, in the following text. The distributions of two meshes are illustrated in Fig. 1. The non-dimensional distance between the first grid point to the surface of the strut,  $y^+$ , varied between 5–36 for mesh A and 3–29 for mesh B. It should be noted that in those simulations,  $y^+$  covers most of the surface particularly near the trailing-edge, which are less than 10 to ensure the proper resolution of the boundary layer. The time-step ( $\Delta t$ ) was 0.00003 s. Fig. 2 illustrates the comparison of the time-averaged pressure distribution along the lifting strut. It can be seen that the results of the two meshes are converged and the overall distributions are in good agreement with the experimental data, although the pressure peak predicted at the leading edge is slightly higher and the secondary peak at the “elbow” location ( $\approx 0.65C$ ) materializes earlier than the experimental measurements. This may be due to the fact that the measurement points were not fine enough to fully capture the pressure distribution at these locations.

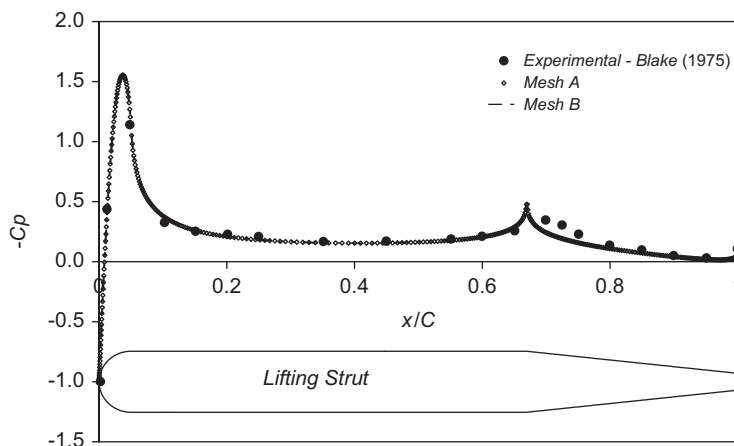


Fig. 2. Time-averaged pressure coefficient distribution for the lifting strut compared to experimental data.

The predicted periodic velocity fluctuations ( $u_{rms}/U_\infty$ ) in the near-wake compared with Blake’s (1975) experimental data are shown in Fig. 3. The magnitudes of the numerical predictions agree with the experimental data reasonably well, except for the second velocity profile closest to the trailing-edge. This could be due to the well accepted fact that the  $\kappa$ - $\epsilon$  model tends to over-predict the turbulence production, hence damping the near-wake structure. The discrepancy between the experimental and numerical results in terms of the shape of the profiles is also observed, in which the experimental data demonstrated asymmetrical patterns about the wake centreline, whereas the current numerical data show perfect symmetrical distributions. This might be due to experimental uncertainties since, for example, a measurement on a symmetrically thick blunt plate with an elliptical leading edge undertaken by Bearman (1965) revealed symmetrical streamwise velocity fluctuating profiles. The comparison of the vertical distances between the local  $u_{rms}/U_\infty$  maxima of each of the profiles in Fig. 3 to the experimental data is given in Fig. 4. The predicted minimum is in excellent agreement with the experimental data. According to Bearman (1965), the location of this minimum corresponds to an intensified velocity fluctuation peak, which marks the end of the wake formation region ( $l_f$ ). It is observed that the computed peaks are more pronounced and closely match the location of this minimum when the streamwise velocity fluctuation profiles are taken at a vertical position away from the centreline (not shown here). Therefore, the profile of  $u_{rms}$  along the streamwise direction at  $y = 0.25$  mm is used to determine the wake formation length ( $l_f$ ) for the results discussed in the following sections. The predicted trailing-edge characteristics are given in Table 2, which are in a good agreement with the experimental data of Blake (1975). It should be noted that the discrepancy between the current prediction and experiments may be the result of the over-prediction of shedding vortex

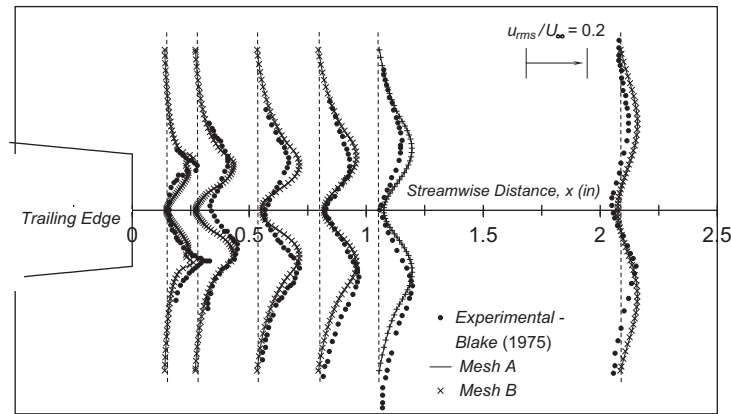


Fig. 3. Comparisons of streamwise velocity fluctuations at various locations aft of the trailing-edge for the lifting strut.

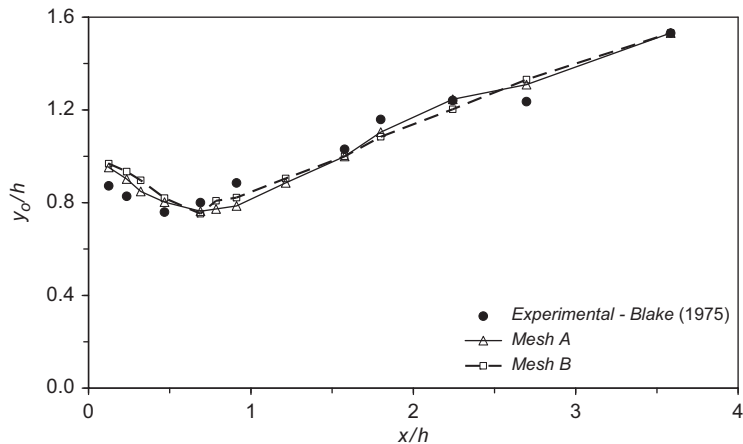


Fig. 4. Numerical predictions of cross-wake distance of the velocity fluctuation maxima  $y_0$  and experimental measurements for the lifting strut ( $x$  is defined as in shown Fig. 3).

strength due to the intrinsic nature of the 2-D simulation, leading to a shorter vortex formation length and higher shedding frequency in the prediction. A 3-D simulation would improve the comparison.

### 3.2. NACA 0015 grid independence and time-step resolution study

A thorough study of the grid and time-step ( $\Delta t$ ) sensitivity was carried out to ensure the solutions of URANS is mesh independent for a particular meshing scheme and discretization time-step size, respectively, before performing the parametric studies on the NACA 0015 section. This task was carried out on the squared-off blunt profile with the most extreme vertical cut at 99% chord of the NACA 0015 hydrofoil. The corresponding blunt trailing-edge height is 3.58 mm and the inflow free-stream velocity is  $U_\infty = 5$  m/s. In developing the computational mesh, care had to be taken in discretizing the near-wake region, where a rich blend of viscous phenomena and unsteady vortical flows exists. Smooth and gradual variations of the cell skewness, cell area as well as cell aspect ratio in this region are vital in limiting the associated numerical errors, hence achieving a good solution of the flow, as illustrated in Fig. 1(b). The non-dimensional distance between the first node point and the surface throughout the entire hydrofoil has to be  $y^+ \leq 1$  to ensure the accurate resolution of the turbulent boundary layer. The time-step  $\Delta t = 0.00005$  s is used to perform the grid independence study.

Three meshes, which gave a constant refinement ratio ( $r$ ) equal to 1.5 defined as  $r = (N_{fine}/N_{coarse})^{1/2}$  with a constant stretching coefficient, were used in the grid convergence study, where  $N$  is the number of grid cells. The summary of the grid convergence is shown in Table 3. The convergences for most variables show an oscillatory behaviour. These behaviours are expected for an upwind-type scheme used in this study (Celik et al., 2005). The uncertainties of the solutions were estimated using the power law method proposed by Celik et al. (2005) and Celik and Karatekin (1997), which is valid for monotonic or oscillatory convergence scenarios. A Grid Convergence Index, GCI, proposed by Roache (1997) and Celik and Karatekin (1997) was used to measure the uncertainty of the solutions. It can be seen from Table 3 that for the finest grid (mesh III), the uncertainty is less than 6% for all variables monitored. According to Roache (1997), an indicator for achieving an asymptotic range is related to the GCI for the coarse grid  $GCI_{21}$ , for the fine grid  $GCI_{32}$ ,  $r$  and the observed order of the accuracy of the numerical scheme  $\alpha$ . It is defined as  $GCI_{21}/(r^\alpha GCI_{32})$ , in which  $\alpha$  is calculated using three grids. A value of the ratio close to one indicates that the asymptotic range is achieved. It can be seen that all variables are converged and are within the asymptotic range. It is reasonable to consider that the

Table 2  
Comparison of various parameters for the lifting strut.

Parameter	Mesh A	Mesh B	Experimental
$l_f/h$	0.79	0.79	0.9
$y_f/h$	0.77	0.81	1.0
$f_s$ (Hz)	366	357	320
$h/\delta^*$	5.80	5.83	5.88
$U_s/U_\infty$	1.03	1.03	1.05
$10 \log_{10}(p_{rms}^2/q_\infty^2)$	-23.66	-23.61	-22.03
$C_d$	0.019	0.018	-

Table 3  
Convergence of the mean and fluctuating parameters for the NACA 0015 grid independence study,  $Re = 3.459 \times 10^6$ .

Mesh	I	II	III	Error <sup>a</sup> (%)	Uncertainty (%)	Asymptotic range
Grid cells	53946	122678	275000			
$C_{d-mean}$	0.01050	0.01028	0.01020	0.47	1.41	1.00
$f_s$	143.49	143.54	139.99	2.09	5.95	1.05
$l_f$	0.983665	0.95799	0.94962	1.81	5.33	1.03
$C_{l-rms}$	0.001428	0.001541	0.001537	0.21	0.63	1.05
$p_{rms}^b$	187.05	198.53	197.72	0.33	2.04	1.04

<sup>a</sup>Error is based on Richardson extrapolation.

<sup>b</sup>The fluctuating static pressures  $p_{rms}$  taken at the top corner of the trailing-edge.

grids (I–III) are within the asymptotic range. The results for mesh III are considered as mesh independent, given that their relative errors based on the Richardson Extrapolation were less than 2%. The subsequent simulations are performed based on the meshing scheme used in mesh III. Each run would require about 250 CPU hours to obtain a statistically steady solution.

Selection of the appropriate time-step size is also crucial in predicting the shedding frequency and capturing the associated unsteadiness in the near-wake. While the residence time approach used for choosing the time-step size produces a reasonable agreement to experimental data for the validation case considered earlier, a time-step size sensitivity study was also carried out to make certain the solution is  $\Delta t$  independent. The results are given in Table 4. It can be seen from the table that the mean drag coefficient ( $C_d$ ) converges to a value of 0.0102 for all  $\Delta t$  values, while  $p_{rms}$  and the shedding frequency vary significantly, only converging when comparing the results of  $\Delta t = 0.00005$  and  $\Delta t = 0.000035$  s. Thus  $\Delta t = 0.00005$  s was chosen as the timestep for simulations with freestream velocities of 5 m/s. Other  $U_\infty$  investigated are 2, 7, 7.5 and 11.5 m/s, and the corresponding time-step sizes for computations are  $\Delta t = 5 \times 10^{-5}$ ,  $\Delta t = 9 \times 10^{-6}$ ,  $\Delta t = 8.5 \times 10^{-6}$  and  $\Delta t = 6 \times 10^{-6}$  s, respectively.

### 3.3. NACA 0015 with a squared-off blunt trailing-edge

The chordwise distribution of the static pressure for the NACA 0015 section is shown in Fig. 5(a) for the suction surface, in which the pressure is non-dimensionalised with freestream dynamic pressure (pressure side not shown due to symmetry). It can be seen that a favourable pressure gradient region exists which peaks with a minimum pressure of  $C_p = -0.5$  at approximately 11% chord, followed by a constant adverse pressure gradient region covering most of the surface up to 90% chord. Although there is a steeper adverse pressure gradient further decelerating the flow from 90% chord to the trailing-edge, no separation was observed for any of the cases investigated. A closer examination of the  $C_p$  distribution near the trailing-edge (Fig. 5(b)) demonstrates that a short region of favourable pressure gradient exists, which starts from 99.8% chord. A similar observation is also reported by Blake (1975) for the squared-off blunt lifting strut, although in his experiment the favourable pressure gradient region starts much earlier, at  $\approx 95\%$  chord and is more pronounced due to the considerably blunter trailing-edge.

Fig. 6 shows the variation of the displacement thickness  $\delta^*$  for the NACA 0015 hydrofoil taken at the trailing-edge compared to the closest geometrically similar profile, the NACA 0012 section. The displacement thickness variation for flow past the NACA 0012 is based on the experimental correlation given by Brooks et al. (1989) for a heavily tripped boundary layer. The current numerical prediction exhibits a similar trend to that of flow past the NACA 0012 section, although the  $\delta^*$  for flow past the NACA 0015 is seen to be consistently smaller. The displacement boundary layer thickness near the trailing-edge as a function of trailing-edge height Reynolds number  $Re_h$  is depicted in Fig. 7. The displacement boundary layer  $\delta^*$  demonstrates a dependency on  $Re_h$  similar to that shown in Fig. 6. It should be noted that each  $\delta^*$  is calculated at a different location because of the change of the trailing-edge geometry in Fig. 7. Given that  $\delta^* = f(x, Re)$  and it increases significantly towards the trailing-edge (see Fig. 8), some degree of non-smoothness in this correlation should be anticipated due to the limited number of simulations. However, the trend is clearly illustrated.

Based on collective results, Blake (1986) concluded that vortex shedding of turbulent flows over rigid hydrofoils will occur when the trailing-edge has a sufficient degree of bluntness, i.e. when the bluntness parameter  $h/\delta^*$  is greater than 0.3. The current numerical investigation of flow over the NACA 0015 hydrofoil with the “sharpest” trailing-edge (where the vertical cut located 99.8% chord) does not exhibit vortex shedding when the freestream velocity is 2 m/s. This corresponds to a bluntness of  $h/\delta^* = 0.55$ . When freestream velocity is increased to 5 m/s (and greater), large scale vortices are detected. A bluntness parameter of  $h/\delta^* = 0.67$  is determined at onset of vortex shedding with a corresponding trailing-edge Reynolds number of  $Re_h = 13\,500$ . The trailing-edge height Strouhal number ( $St_h = f_s h / U_\infty$ ) as a function of  $Re_h$  is given in Fig. 9. It shows a second-order dependency on  $Re_h$  according to this study.

Table 4

Summary of mean and fluctuating parameters of mesh III (with  $U_\infty = 5$  m/s) for NACA 0015 time-step size resolution study.

$\Delta t$ (s)	0.001	0.0005	0.0001	0.00005	0.000035
$C_{d\text{-mean}}$	0.0103	0.0103	0.0102	0.0102	0.0102
$p_{rms}$ (Pa)	91	121	205	197	196
$f_s$ (Hz)	28	51	123	140	143



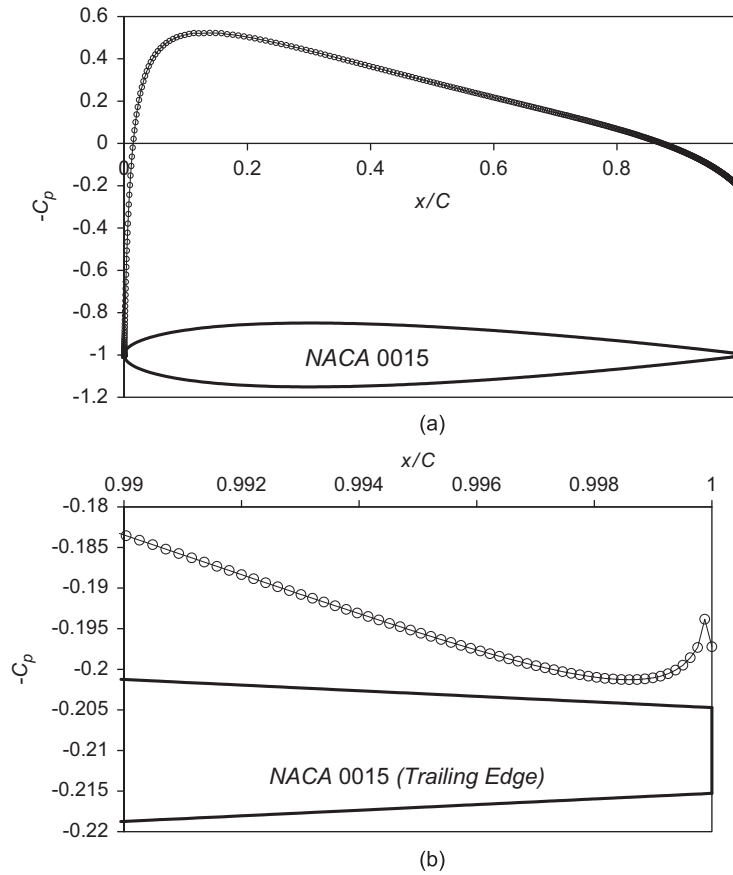


Fig. 5. Static pressure distribution over the NACA 0015 hydrofoil: (a) complete distribution and (b) trailing-edge distribution.

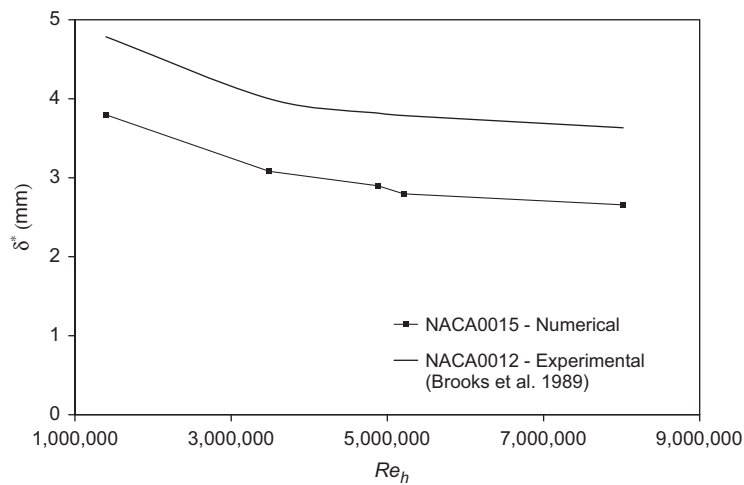


Fig. 6. Numerical prediction of the variation of trailing-edge displacement thickness with Reynolds number.

Based on the extensive review of various experimental studies with different trailing-edge solid angles  $\psi$  (the angle between the sloping surfaces upstream of the trailing-edge) and their bluntness parameters,  $h/\delta^*$ , including Blake's (1975) study, a relationship between the trailing-edge height Strouhal number ( $St_h = fh/U_\infty$ ) and the characteristics of

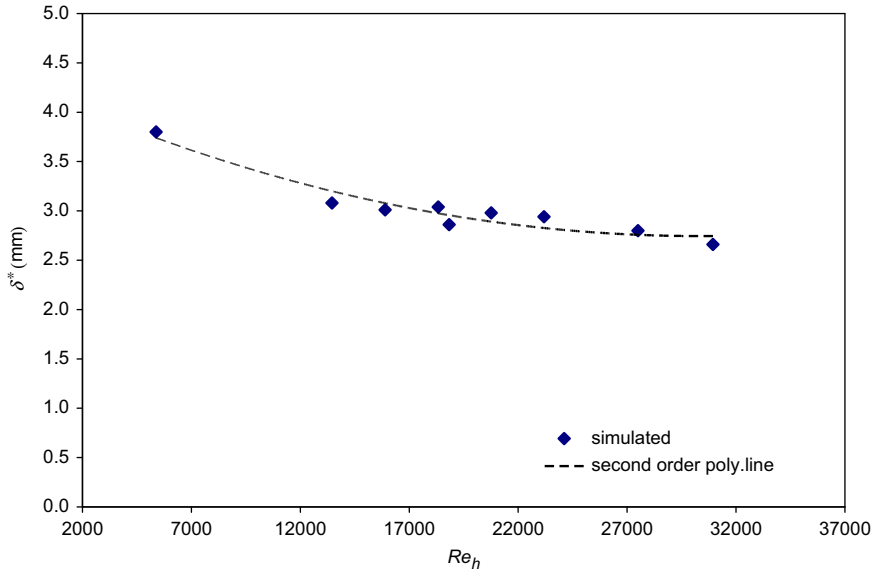


Fig. 7. Displacement boundary layer thickness as a function of trailing-edge Reynolds number.

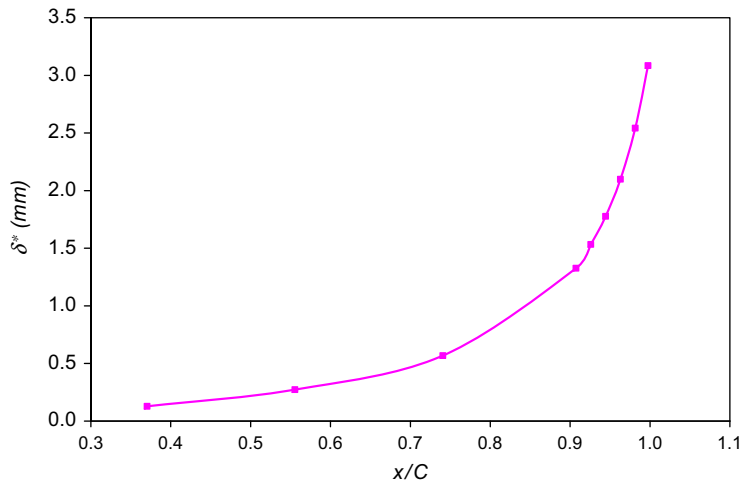


Fig. 8. Predicted displacement boundary layer thickness as a function of locations along the cord.

the trailing-edge flow is proposed by Brooks et al. (1989) as

$$St_h = \frac{0.212 - 0.0045\psi}{1 + 0.235(h/\delta^*)^{-1} - 0.0132(h/\delta^*)^{-2}} \tag{1}$$

Given that the trailing-edge solid angle,  $\psi$ , for the NACA 0015 hydrofoil studied is approximately  $19.6^\circ$ , a comparison of the current numerical prediction to the results of Eq. (1) is shown in Fig. 10. An average 10% deviation is achieved across the range of bluntness parameters examined for the current numerical prediction using URANS. The predicted  $St_h$  is around 0.08–0.1. The numerical results shown here confirm Eq. (1), that is the Strouhal number increases with an increase of the non-dimensional trailing-edge bluntness  $h/\delta^*$ . To explain the non-smooth nature of the simulation results given in Fig. 10, we plot the  $h/\delta^*$  as a function of  $Re_h$  shown in Fig. 11. It reveals a highly non-linear relationship between those two variables, while good behaviours of the displacement boundary layer thickness  $\delta^*$  versus  $Re_h$  and  $x/C$  are achieved, as shown in Figs. 7 and 8. A non-linear relationship between the Strouhal number  $St_h$  and

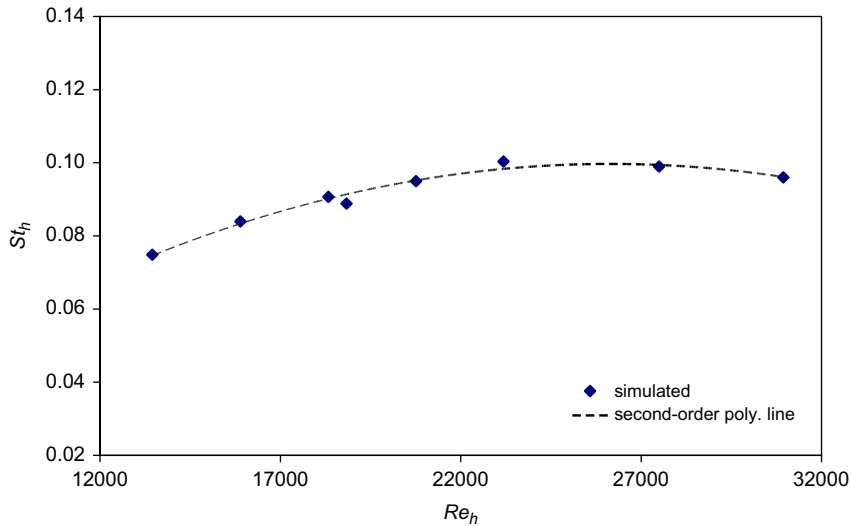


Fig. 9. Trailing-edge height based Strouhal number as a function of trailing-edge-based Reynolds number.

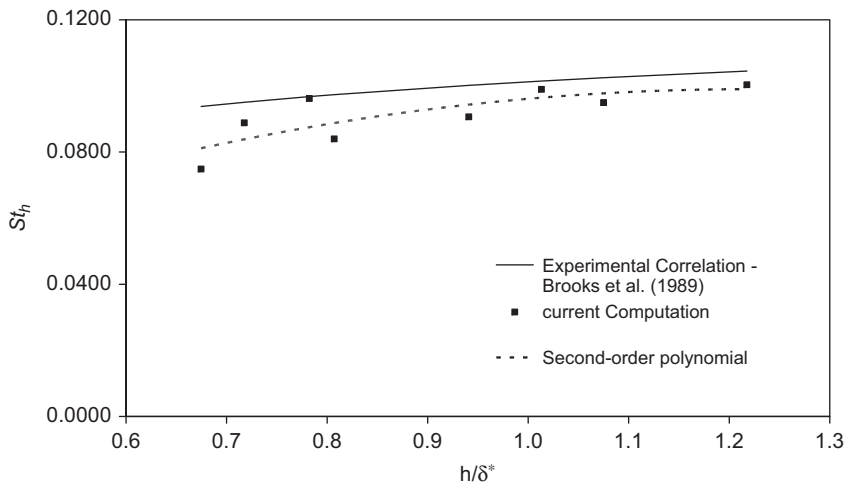


Fig. 10. Comparison of the predicted Strouhal number for the squared-off trailing-edge NACA 0015 hydrofoil with varying trailing-edge bluntness parameters.

the non-dimensional bluntness ( $h/\delta^*$ ) should be expected. However, it seems that there is a lower-ordered approximate correlation between  $St_h$  and  $Re_h$  as shown in Fig. 9, and it should serve well for engineering applications. It means that for a given trailing-edge geometry, the trailing-edge height based  $St_h$  could be estimated using  $Re_h$  without a comprehensive knowledge of the flow if there is a vortex shedding.

The effect of Reynolds number on the wake formation region is illustrated in Fig. 12. Due to the lack of experimental data for the hydrofoil studied, the present numerical findings are compared to the data of flows over the circular cylinder by Bloor (1964) in a similar range of Reynolds number. It can be seen from Fig. 12 that the non-dimensional formation region is shortened and reaches a near-constant value of 0.9 with an increase in  $Re_h$ . This agrees with the many experimental data (e.g. Blake, 1986). On the other hand, the cross-wake shear layer thickness,  $y_f$ , does not vary much with  $Re_h$  and attained an average value of 0.66, as shown in Fig. 12. This demonstrates that it is acceptable to use either  $y_f$  or  $h$  to define the Strouhal number for trailing-edge vortex shedding. The Strouhal number based on the cross-wake shear layer thickness is about 0.36–0.47.

The occurrence of vortex shedding often causes the near-wake fluid to rapidly circulate and constantly change direction due to the alternate roll-up of the shear layer. This unsteady chaotic mixing of the fluid induces a pressure

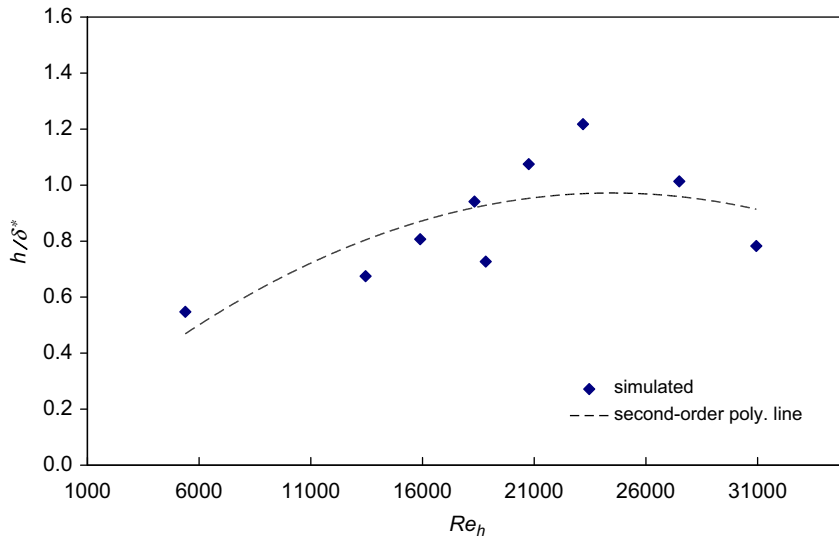


Fig. 11. The irregular characteristics of non-dimensional bluntness as a function of trailing-edge height based Reynolds number.

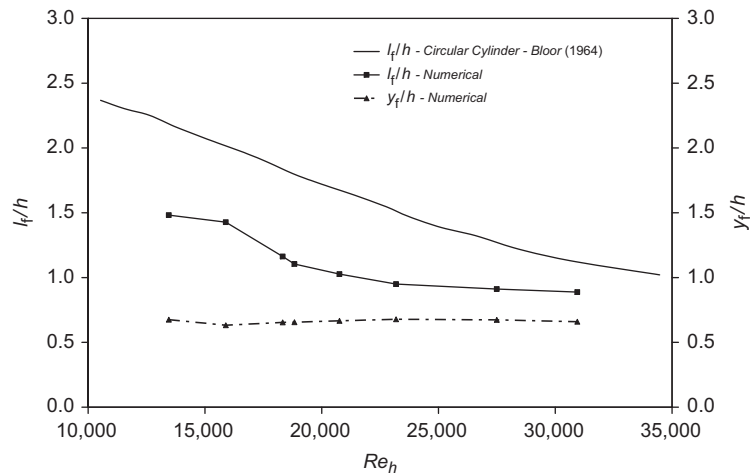


Fig. 12. Variation of wake formation lengths and cross-wake thickness with trailing-edge Reynolds number, for the squared-off NACA 0015 section.

differential across the surface of the hydrofoil, which reaches a maximum at the trailing-edge (Blake, 1986). Fig. 13 illustrates the effects of  $Re_h$  and non-dimensional formation length  $l_f/h$  on the maximum fluctuating pressures non-dimensionalised by the freestream dynamic pressure  $q_\infty$ ,  $10\log_{10}(p_{rms}^2/q_\infty^2)$ . It can be seen that the fluctuation pressure increases with an increase of  $Re_h$  (Fig. 13(a)) and decreases with the reduction of the formation region  $l_f/h$  (Fig. 13(b)). The increase in the fluctuating pressure is caused by the higher-strength vortices formed in the near-wake for the blunter trailing-edge or a shorter formation region. This is evident in Fig. 14 and where the vorticity magnitude of the newly shed vortex for the blunter profile is higher at the core of Fig. 14(b), almost doubling the magnitude compared to that of the newly shed vortex for the sharper trailing-edge of Fig. 14(a). According to Blake (1986), the trailing-edge noise is closely related to the turbulence or fluctuation pressure near the trailing-edge, the higher fluctuation pressure would lead to the production of higher-intensity acoustic noise. Moreover, it is generally known that the “bound” circulation  $\Gamma$  about the vortex producing body, which is responsible for the production of the lift force, is constantly changing and should be ideally equal to the circulation strength of the shed vortex (Heskestad and Olberts, 1960). Also, the circulation is directly proportional to the vorticity. Thus the higher vorticity produced by the flow over the blunter

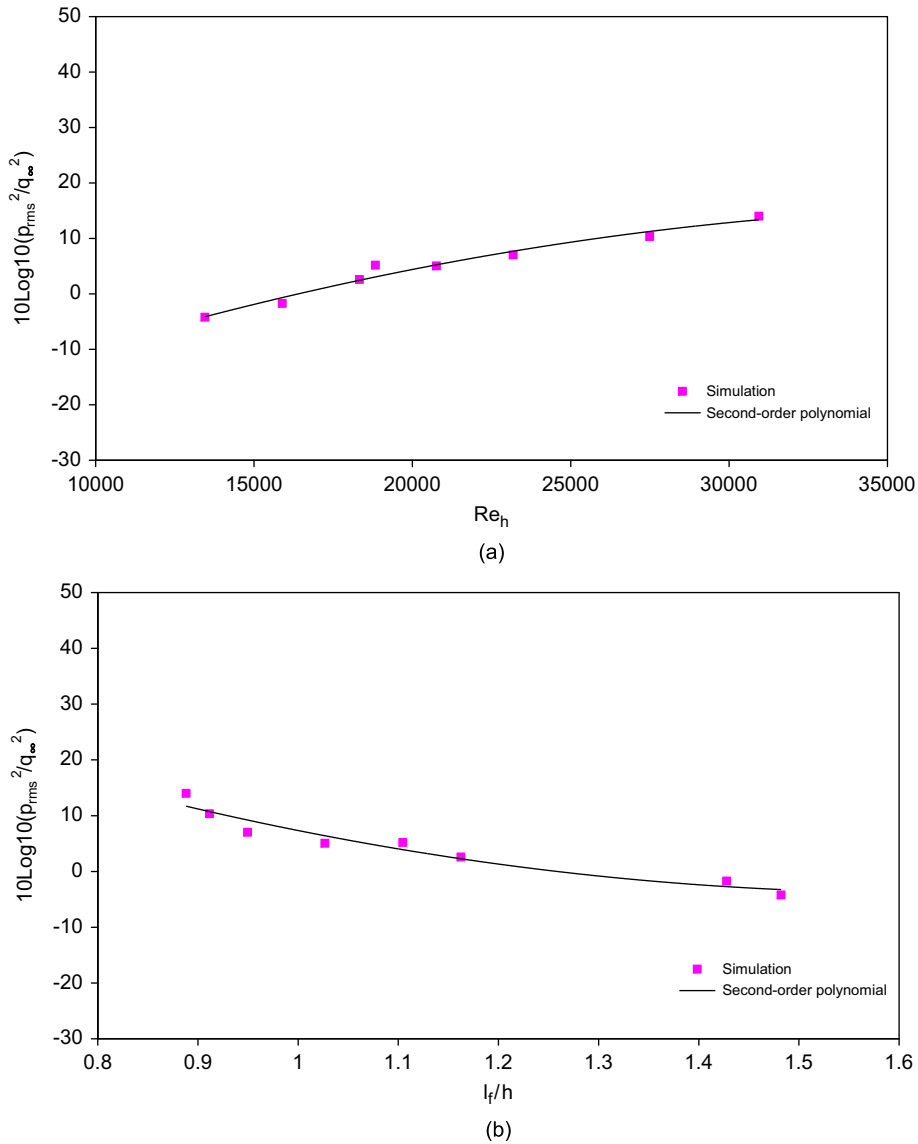


Fig. 13. Effects of trailing-edge-based Reynolds number and formation length on the trailing-edge fluctuating pressure for NACA 0015 squared-off trailing-edge: (a) effect of trailing-edge Reynolds number and (b) effect of non-dimensional formation length.

profile results in a dramatic increase in the fluctuating lift coefficient  $C_{l-rms}$ , e.g. 0.00036 and 0.00119 for the “sharp” and blunt profiles, respectively, leading to a stronger dipole sound.

#### 3.4. NACA 0015 with trailing-edge cavities

Modifications of the trailing-edge configurations were applied at 99% chord of the original sharp-edged NACA 0015 section, resulting in a trailing-edge height of  $h = 3.58$  mm. A summary of the various characteristics of different configurations compared to the squared-off blunt trailing-edge is given in Table 5. To further investigate whether the shape or the area size of the cavity ( $A_c$ ) have an impact on near-wake flows, the cavity base of profile *D* was placed at various depths within the section (towards the leading edge) to achieve more cavity area. Profiles *D1* and *D3* (see Table 5) have the same cavity areas  $A_c$  as those of profiles *B* and *C*, respectively. Parameterisation is obtained by non-dimensionalising the cavity area  $A_c$  to the reference area  $A_h$ . This reference area is enclosed by a hypothetical square with sides equal to the height of the trailing-edge  $h$ .



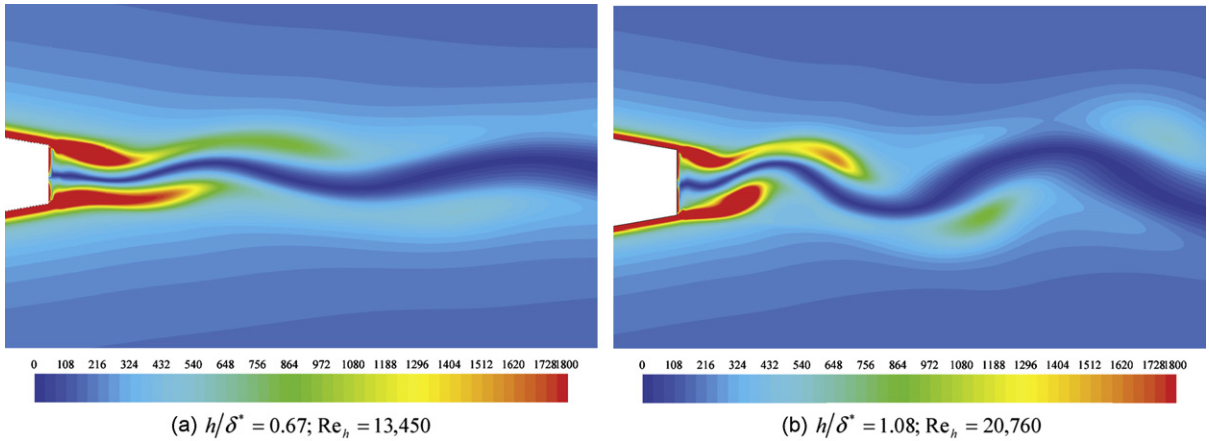



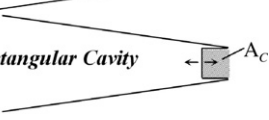


Fig. 14. Trailing-edge instantaneous vorticity contours (1/s) for NACA 0015: (a) “sharp” and (b) blunt trailing-edge.

Table 5

Comparison of various characteristics of different trailing-edge configurations for the NACA 0015 section with  $Re = 3.459 \times 10^6$ .

Profile	$A_c/A_h$	$C_d$	$h/\delta^*$	$l_f/h$	$f_s$ (Hz)	$10 \log(P_{rms}^2/q_\infty^2)$	
<b>A</b> <i>Squared-off Blunt</i> 	–	<b>0.0102</b>	<b>1.22</b>	<b>0.95</b>	<b>140</b>	<b>7.02</b>	
<b>B</b> <i>90° Triangular Cavity</i> 	<b>0.25</b>	<b>0.0102</b>	<b>1.21</b>	<b>1.13</b>	<b>146</b>	<b>1.82</b>	
<b>C</b> <i>Semi-Circular Cavity</i> 	<b>0.39</b>	<b>0.0102</b>	<b>1.20</b>	<b>1.04</b>	<b>144</b>	<b>–0.96</b>	
<b>D</b> <i>Rectangular Cavity</i> 	<b>1</b>	<b>0.25</b>	<b>0.0103</b>	<b>1.21</b>	<b>1.07</b>	<b>144</b>	<b>0.69</b>
	<b>2</b>	<b>0.33</b>	<b>0.0103</b>	<b>1.21</b>	<b>1.11</b>	<b>146</b>	<b>–0.63</b>
	<b>3</b>	<b>0.39</b>	<b>0.0102</b>	<b>1.21</b>	<b>1.14</b>	<b>145</b>	<b>–1.22</b>
	<b>4</b>	<b>0.50</b>	<b>0.0103</b>	<b>1.21</b>	<b>1.14</b>	<b>147</b>	<b>–1.78</b>
	<b>5</b>	<b>0.67</b>	<b>0.0103</b>	<b>1.21</b>	<b>1.14</b>	<b>147</b>	<b>–2.13</b>
	<b>6</b>	<b>1.18</b>	<b>0.0103</b>	<b>1.22</b>	<b>1.14</b>	<b>146</b>	<b>–2.35</b>

Note:  $P_{rms}$  is taken at location  $x/h = 0.11$ .

The mean drag coefficient and the bluntness parameter, as shown in Table 5, are not affected by the presence of the different trailing-edge profiles. In addition, the mean base pressure coefficient at  $x/C = 1$  (not shown) is also found to be unchanged. The results of Table 5 also imply that the shedding frequency is insensitive to the application of different cavity profiles. This agrees with the observation made by Hestestad and Olberts (1960) and Toebes and Eagleson (1961). Hestestad and Olberts (1960) observed that the shedding frequency of a squared-off blunt trailing-edge was the same as that of the same section with a semicircular cavity, and Toebes and Eagleson (1961) found that the shedding frequency of a squared-off blunt trailing-edge was slightly lower than that of the same section with a 90° triangular trailing-edge. However, the numerical predictions of the shedding frequency for the rectangular cavity profiles do not fully agree with Zhdanov and Eckelmann’s experiment (1994), where they found that the Shoudal number increased with an increase in the base depth up to  $A_c/A_h = 0.7$  for a thick flat pate having a circular leading edge. The numerical predictions show an increase in frequency with an increase of the cavity depth up to  $A_c/A_h = 0.5$ , and a further increase

in the base depth has little effect on the shedding frequency. As it has been shown above, the vortex shedding is very sensitive to the non-dimensional bluntness,  $h/\delta^*$ . The lack of detailed experimental data of the turbulent boundary layer may be the main reason leading to the discrepancy. The total radiated sound power from the foil can be calculated using Curle's integral acoustic analogy. The contribution by trailing-edges can be estimated using the same analogy, which is directly related to the surface pressure fluctuation and turbulence statistics of boundary layers. The contribution is shown in Table 5. While the sound sources generated by the pressure and suction surfaces maintain almost constant, the dipole contribution from the trailing-edge is significantly affected by the presence of the cavities. Table 5 shows there is a reduction of 5–9 dB in the maximum fluctuation pressure when comparing the section with a cavity (profiles B, C and D) to the squared-off blunt section (profile A). Further, for a particular trailing-edge profile, as the cavity area  $A_c/A_h$  is increased, the maximum fluctuation pressure consistently decreases in magnitude, reaching its asymptotic at  $A_c/A_h = 0.67$  (profile D5). Further increasing and even doubling the cavity area to  $A_c/A_h = 1.18$  (profile D6) seems to have little effect on the maximum fluctuation pressure. A trailing-edge with a cavity will therefore result in a weaker wake than that of a squared-off trailing-edge. This will lead to a reduction of the total dipole sound power contributed by the trailing-edge.

The instantaneous path-lines of fluid flow about the different trailing-edge configurations, coloured by vorticity magnitudes, are depicted in Fig. 15. For the profiles with a base cavity, it can be seen that at onset of roll-up of the vortices, the trapped fluid is gradually drawn into a swirling motion, including the fluid at the very back of the cavity base. The bigger the cavity area, the more the fluid is sucked into this rotational motion, with the sense of rotation dictated by the direction of the forming eddy. This is clearly seen for the profile with a rectangular cavity, profile D5 ( $A_c/A_h = 0.67$ ), as shown in Fig. 15(d). The swirling direction is reversed when the forming vortex sheds and a new one develops. These numerical results confirm Hestekstad and Olberts' (1960) observation and verify that the net circulation behind the trailing-edge needs to be reduced to account for the changing of the rotational sense of the trapped fluid caused by the preceding vortex; hence the bound circulation strength is also lowered to meet the zero net circulation condition. In addition, the reduced bound circulation is further reflected by a significant decrease in the root-mean-square lift coefficient  $C_{l-rms}$  of the two-dimensional section, which decreases with an increase in the cavity area as shown in Fig. 16. For  $A_c/A_h = 0.5$ , a reduction of 61.6% in lift force relative to the squared-off blunt profile has been obtained.

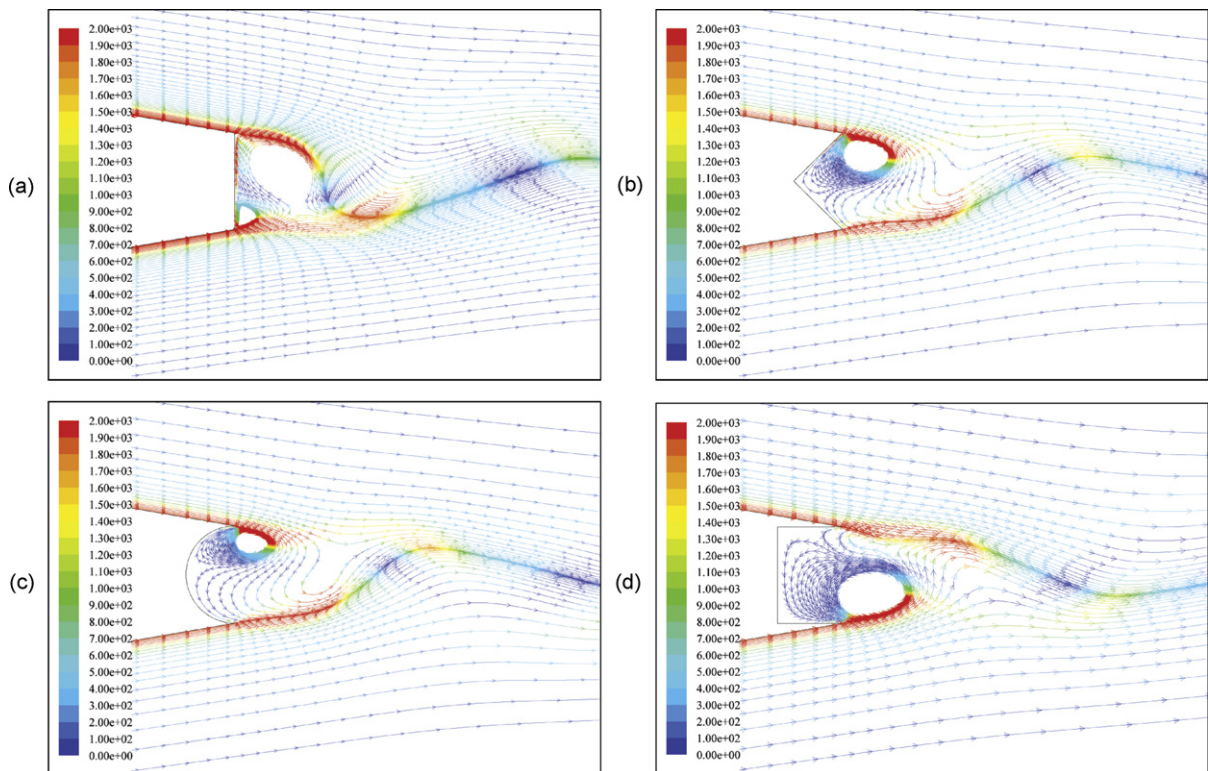


Fig. 15. Instantaneous path-lines of trailing-edge flow of NACA 0015 at  $Re = 3.459 \times 10^6$ : (a) squared-off, (b)  $90^\circ$  triangular cavity, (c) semicircular cavity and (d) rectangular cavity profile. Coloured by vorticity magnitudes (1/s).

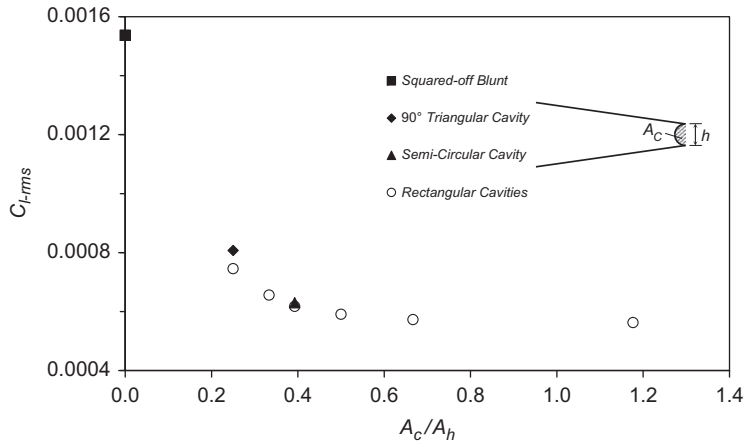


Fig. 16. Effect of increasing cavity area on lift fluctuations, NACA 0015.

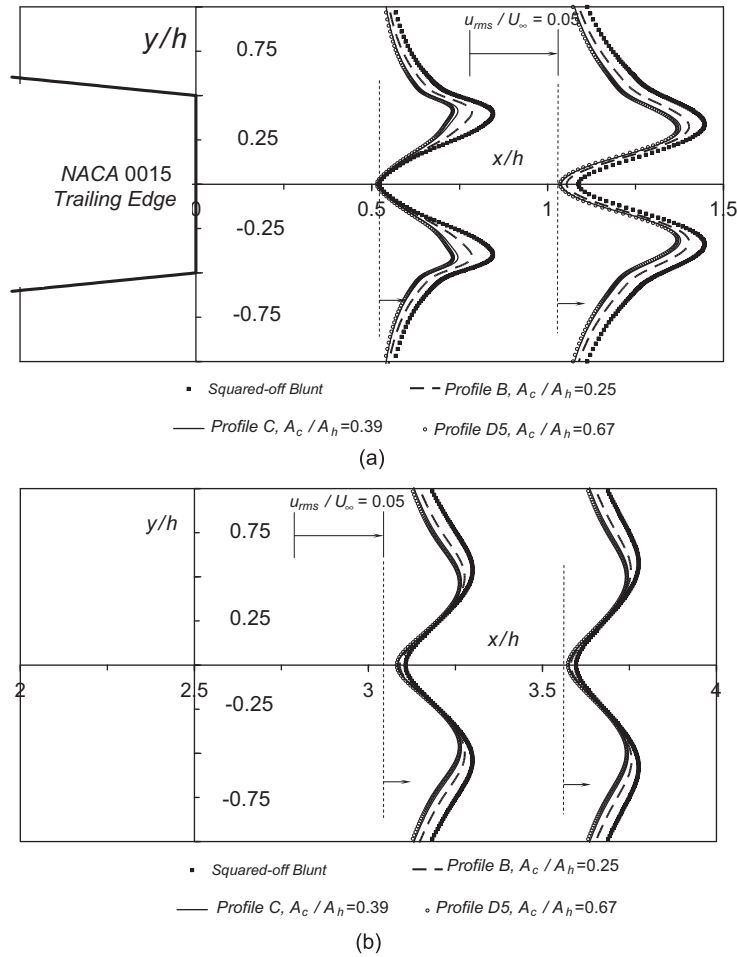


Fig. 17. Streamwise velocity fluctuations taken along the vertical direction in the: (a) near-wake and (b) far-wake aft of the trailing-edge, NACA 0015.

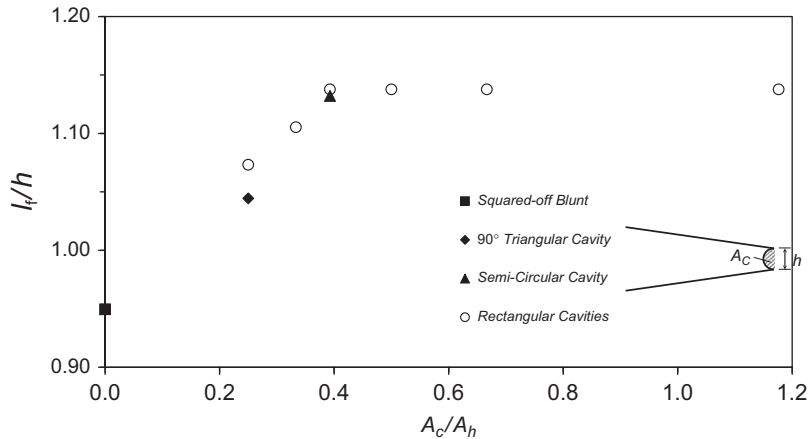


Fig. 18. Effect of increasing cavity area on wake formation lengths, NACA 0015.

It is generally known that the fluctuation of  $C_l$  is directly related to vortex-induced vibrations (Anagnostopoulos, 2002), thus a reduction in this parameter would lead to reduced flow-induced vibrations. Likewise, this reduction in  $C_{l-rms}$  further explains why Heskestad and Olberts (1960) finds a reduction in the relative vibration amplitude of 69% when comparing a 2D section with a semicircular cavity to one with a squared-off blunt trailing-edge.

The existence of the cavity at the trailing-edge induces a weaker wake, which results in a reduction of the near- and far-wake streamwise velocity fluctuations, as demonstrated in Fig. 17. It can be seen that  $u_{rms}/U_\infty$  (taken along the vertical direction) for the 90° triangular, semicircular and the rectangular cavity consistently decreases in value with an increase in  $A_c/A_h$  at both near- and far-wake regions aft of the trailing-edge. At  $x/h = 0.5$ , the velocity fluctuations are significantly affected by the presence of the trailing-edge cavity in the shear layer regions where the flow has just come off the top and bottom trailing-edge corners ( $y/h \approx \pm 0.5$ ). These regions are also the locations of the initial core of the forming vortices (see Fig. 15). Further downstream at  $x/h = 1$ , the streamwise velocity fluctuations are uniformly reduced across the wake region. In the far-wake, the decay of the wake strength is noticeable along the centreline and outside the shear layer. These results confirm that the vortex circulation strength has been compromised by moving an additional amount of the local fluid with the presence of the cavity, thus causing less unsteady fluctuation in the near-wake aft of the trailing-edge. Moreover, as shown in Fig. 18, the vortex formation length increases with an increase in the ratio of  $A_c/A_h$ , which suggests that the weaker streamwise velocity fluctuation causes the delay of the formation of the fully developed vortex.

It is obvious that applying a cavity at the trailing-edge of a two-dimensional section has a noticeable effect on the near-wake fluctuating properties and the lift coefficient. However, it seems that it is cavity area rather than cavity shape that play an important role in altering the wake dynamics. When comparing mean square fluctuating pressure, fluctuating lift coefficient and wake formation length given in Table 5, Figs. 16 and 18, respectively, for different cavity shapes that have the same cavity area (profiles B & D1 and profiles C & D3), it can be seen that the difference is consistently negligible for each of these profile pairs. Further, the variation of these properties with respect to cavity area follows a uniform distribution, again suggesting that cavity size rather than its shape that has more impact on the local flow.

#### 4. Conclusions

Numerical simulations using URANS have been conducted to study two-dimensional turbulent flows over hydrofoils with different blunt trailing-edge configurations. Assessment of the application of the unsteady *realisable*  $\kappa$ - $\epsilon$  model to periodic flows over the trailing-edge shows that a satisfactory agreement is achieved for both the time-averaged and fluctuating parameters of interests in the near-wake. Differences in the prediction of the streamwise velocity fluctuation magnitudes are observed which may be due to 3-D effects; nonetheless, the vortex formation length and the location of the fully developed vortex core which corresponds to the peak in the velocity fluctuation are computed with acceptable accuracy. It seems that the application of URANS combined with a conventional acoustic analogy to predict the tonal noise induced by a high Reynolds number lifting-surface-flow will be a very promising approach. It can also be used in

engineering applications where a vortex-induced vibration is concerned and the optimisation of a design is required. Due to its lower computing cost, the prediction of a two-way coupled fluid–structure interaction is possible.

Parametric study of the flows past the squared-off blunt hydrofoil with different bluntness parameters shows that the numerical prediction of the Strouhal numbers matches that of experimental correlations satisfactorily. Consistent increases of the mean-square pressure fluctuations and the intensity of the vortex strengths at the trailing-edge are observed when the degree of bluntness is amplified.

The existence of a base cavity at the trailing-edge does not change the inherent Strouhal number of the two-dimensional section examined as long as the characteristic trailing-edge height remains the same. However, the existence of the cavity decreases the intensity of the trailing-edge pressure fluctuations and consequently results in a reduction of lift fluctuations. It also plays a part in easing the turbulence intensity in the immediate wake region and results in an extended wake-formation region. It is observed that the area of the cavity has more influence on the trailing-edge wake dynamics than its shape does.

As it may be well accepted that a 2-D simulation will always over-predict the strength of the shedding vortex thus the shedding frequency at some extent due to its intrinsic limitation, the more accurate results could be achieved on a full 3D simulation. This is under investigation.

### Acknowledgements

This study is sponsored by Australian Postgraduate Awards (APA) from the Australian Government; the School of Aerospace, Mechanical and Manufacturing Engineering at RMIT University and the Defence Science & Technology Organisation (Australia) through a research agreement.

### References

- Anagnostopoulos, P., 2002. In: *Flow-Induced Vibrations in Engineering Practice*. WIT Press, UK.
- Bearman, P.W., 1965. Investigation of the flow behind a two-dimensional model with a blunt trailing edge and fitted with splitter plates. *Journal of Fluid Mechanics* 21 (2), 241–255.
- Blake, W.K., 1975. Periodic and random excitation of streamlined structures by trailing edge flows. In: *Proceedings of the Fourth Biennial Symposium on Turbulence in Liquids*, Rolla, MO, USA.
- Blake, W.K., 1976. A near-wake model for the aerodynamic pressures exerted on singing trailing edges. *Journal of the Acoustical Society of America* 60 (3), 594–598.
- Blake, W.K., Maga, L.J., Finkelstein, G., 1977. Hydroelastic variables influencing propeller and hydrofoil singing. In: *Proceedings of the ASME Symposium on Noise of the Fluids Engineering Division*, Atlanta, GA, USA, pp. 191–200.
- Blake, W.K., 1986. *Mechanics of Flow-Induced Sound and Vibration*, vols. I and II. Academic Press, Orlando.
- Bourgoyne, D.A., Ceccio, S.L., Dowling, D.R., Jessup, S., Park, J., Brewer, W., Pankajakshan, R., 2000. Hydrofoil turbulent boundary layer separation at high Reynolds number. In: *Proceedings of the 23rd Symposium on Naval Hydrodynamics*, Val de Reuil, France.
- Bourgoyne, D.A., Hamel, J.A., Ceccio, S.L., Dowling, D.R., 2003. Time averaged flow over a hydrofoil at a high Reynolds number. *Journal of Fluid Mechanics* 496, 365–404.
- Bourgoyne, D.A., Ceccio, S.L., Dowling, D.R., 2005. Vortex shedding from a hydrofoil at a high Reynolds number. *Journal of Fluid Mechanics* 531, 293–324.
- Brooks, T.F., Pope, D.S., Marcolini, M.A., 1989. *Airfoil self-noise and prediction*. NASA Reference Publication, 1218.
- Bloor, S.M., 1964. The transition to turbulence in the wake of a circular cylinder. *Journal of Fluid Mechanics* 51, 233–272.
- Carlson, J.R., Duquesne, N., Rumsey, C.L., Gatski, T.B., 2001. Computation of turbulent wake flows in variable pressure gradient. *Computers and Fluids* 30, 161–187.
- Celik, I., Li, J., Hu, G., Shaffer, C., 2005. Limitation of Richardson extrapolation and some possible remedies. *ASME Journal of Fluids Engineering* 127 (September), 795–805.
- Celik, I., Karatekin, O., 1997. Numerical experiments on application of richardson extrapolation with nonuniform grids. *ASME Journal of Fluids Engineering* 119, 584–590.
- Date, J.C., Turnock, S.R., 2002. Computation evaluation of the periodic performance of a NACA0012 fitted with a gurney flap. *ASME Journal of Fluids Engineering* 124, 227–234.
- Donaldson, R.M., 1956. Hydraulic-turbine runner vibration. *ASME Journal of Fluids Engineering* 78, 141–1147.
- Gershfeld, J.L., Blake, W.K., Knisely, C.W., 1988. Trailing edge flows and aerodynamic sound. In: *Proceedings of the First Fluid Dynamics Conference*, Cincinnati, OH.
- Heskestad, G., Olberts, D.R., 1960. Influence of trailing edge geometry on hydraulic-turbine-blade vibration resulting from vortex excitation. *ASME Journal of Engineering for Power* 82, 103–110.



- Howe, M.S., 1991. Aerodynamic noise of a serrated trailing edge. *Journal of Fluids and Structures* 5, 33–45.
- Howe, M.S., 1999. Trailing edge noise at low Mach numbers. *Journal of Sound and Vibration* 225, 211–238.
- Howe, M.S., 2000. Trailing edge noise at low Mach numbers, Part 2: attached and separated flows. *Journal of Sound and Vibration* 234, 761–765.
- Howe, M.S., 2001. Unsteady lift and sound produced by an airfoil in a turbulent boundary layer. *Journal of Fluids and Structures* 15 (2), 207–225.
- Iaccarino, G., Ooi, A., Durbin, P.A., Behnia, M., 2003. Reynolds averaged simulation of unsteady separated flow. *International Journal of Heat Fluid Flow* 24, 147–156.
- Mathey, F., 2008. Aerodynamic noise simulation of the flow past an airfoil trailing-edge using a hybrid zonal RANS-LES. *Computers and Fluids* 37, 836–843.
- Mulvany, N., Tu, J.Y., Chen, L., Anderson, B., 2004. Assessment of two-equation turbulence modelling for high Reynolds number hydrofoil flow. *International Journal of Numerical Methods in Fluids* 45, 275–299.
- Nguyen, P., Gorski, J., 1991. Navier–Stokes analysis of turbulent boundary layer wake for two-dimensional lifting bodies. In: *Proceedings of the Eighteenth Symposium on Naval Hydrodynamics*, Ann Arbor, USA, pp. 633–643.
- Patel, V., Scheuerer, G., 1982. Calculation of two-dimensional near and far wakes. *AIAA Journal* 20 (7), 900–907.
- Patel, V., Chen, H., 1987. Turbulent wake of a flat plate. *AIAA Journal* 25 (8), 1078–1085.
- Paterson, E.G., Peltier, L.J., 2005. Detached-eddy simulation of high-Reynolds-number beveled-trailing-edge boundary layers and wakes. *ASME Journal of Fluids Engineering* 127, 897–906.
- Poirel, D., Yarris, Y., Benaissa, A., 2008. Self-sustained aeroelastic oscillations of a NACA0012 airfoil at low-to-moderate Reynolds numbers. *Journal of Fluids and Structures* 24 (5), 700–719.
- Rani, H.P., Sheu, T.W.J., Tsa, E.S.F., 2007. Eddy structures in a transitional backward-facing step flow. *Journal of Fluid Mechanics* 588, 43–58.
- Roache, P., 1997. In: *Verification and Validation in Computational Science and Engineering*. Hermson Publisher.
- Rodi, W., 1993. On the simulation of turbulent flow past bluff bodies. *Journal of Wind Engineering and Industrial Aerodynamics* 46–47, 3–19.
- Rumsey, C.L., Ying, S.X., 2002. Prediction of high lift: review of present CFD capability. *Progress in Aerospace Sciences* 38, 145–180.
- Shaw, C.T., 1992. In: *Using Computational Fluid Dynamics*. Prentice Hall, New York.
- Toebes, G.H., Eagleson, P.S., 1961. Hydroelastic vibrations of flat plates related to trailing edge geometry. *ASME Journal of Basic Engineering* 83, 671–678.
- Tummers, M.J., Hanjalic, K., Passchier, D.M., Henkes, R.A.W.M., 2007. Computations of a turbulent wake in a strong adverse pressure gradient. *International Journal of Heat Fluid Flow* 28 (3), 418–428.
- Wang, M., Moin, P., 2000. Computation of trailing-edge flow and noise using large-eddy simulations. *AIAA Journal* 38, 2201–2209.
- Williamson, C.H.K., 1996. Vortex dynamics in the cylinder wake. *Annual Review of Fluid Mechanics* 28, 477–539.
- Yang, H., Chen, H.C., Han, J.C., Moon, H.K., 2008. Numerical study of film cooled rotor leading edge with tip clearance in 1–1/2 turbine stage. *International Journal of Heat and Mass Transfer* 51, 3066–3081.
- Yao, Y.F., Savill, A.M., Sandham, N.D., Dawes, W.N., 2002. Simulation and modelling of turbulent trailing edge flow. *Flow, Turbulence and Combustion* 68, 313–333.
- Zhdanov, V.L., Eckelmann, H., 1994. Specific features of wake flow behind a two-dimensional body with a cavity on its rear edge. *Journal of Engineering Physics and Thermodynamics* 66, 225–228.